JCTC Journal of Chemical Theory and Computation

A Potential Energy Function for Heterogeneous Proton-Wires. Ground and Photoactive States of the Proton-Wire in the Green Fluorescent Protein

Oriol Vendrell,[†] Ricard Gelabert,*[,‡] Miquel Moreno,[‡] and José M. Lluch[‡,§]

Departament de Química and Institut de Biotecnologia i de Biomedicina, Universitat Autònoma de Barcelona, 08193 Bellaterra (Barcelona), Spain, and

Theoretische Chemie, Physikalisch-Chemisches Institut, Universität Heidelberg, Im Neuenheimer Feld 229, 69120 Heidelberg, Germany

Received March 5, 2008

Abstract: In this paper an EVB-based method to describe the energetics of operation of arbitrary-length heterogeneous proton-wires is described. The method keeps the number of fittable parameters low by exploiting the idea of "protonation states". The method is applied to describe the 3-proton proton-wire described in Green Fluorescent Protein (GFP), and two sets of parameters have been obtained, one for the electronic ground state and another for the photoactive excited electronic state, of a chemical model including the groups supporting the proton-wire and based on CASPT2//CASSCF quality reference energies. The fitted EVB functions are analyzed in static terms. In this way, it is seen that only a minimum exists in S_0 while two exist in S_1: one for the photoproduct and one for the reactant in the excited state, even though consideration of the Franck−Condon excitation energy predicts an effective barrier under 1 kcal mol^{-1}. Topological analysis of the transition state structure reveals a concerted but asynchronous motion of the protons, where the chromophore's proton lags behind, and the final proton of the wire that goes from Ser205 to Glu222 leads the process. Inclusion of nuclear dynamic efects causes this small effective barrier to vanish and predicts an essentially barrierless process in the excited state.

Introduction

Proton transfer is perhaps the single most important and ubiquitous process in chemistry and biochemistry. In a proton transfer process, a hydrogen atom bound to an electronegative atom and thus, with a local positive charge density, transfers and binds to a neighboring electronegative atom with electron lone pairs available. The structural properties of some molecules or residues which are able to act both as proton donors and proton acceptors make it possible that, under certain circumstances, large hydrogen bond networks can be created. This is the case in bulk protic solvents like water, where an extensive hydrogen-bonded network exists that connects neighboring solvent molecules. When such extensive hydrogen-bonded networks come into existence, proton transfer over large distances occurs as a series of single proton transfer processes, either concerted or stepwise, in which several protons move a single step each in the network. This is part of the well-known Grotthuss mechanism of proton transfer in bulk water[1] and explains, for instance, why the transport of protons is generally much faster in liquid water than that of other cations or anions of similar charge and size to the hydronium cation, the smallest hydrated form of proton stable in water.

Theoretical methods have become invaluable tools to understand how enzyme reactions work.[2–4] In recent years proton transfer, and especially proton transfer along a

* Corresponding author e-mail: ricard.gelabert@uab.cat.
[†] Universität Heidelberg.
[‡] Departament de Química, Universitat Autònoma de Barcelona.
[§] Institut de Biotecnologia i de Biomedicina, Universitat Autònoma de Barcelona.

10.1021/ct800075w CCC: $40.75
Published on Web 06/18/2008

sequential arrangement of proton donors and acceptors, the so-called "proton wires," "proton relays", or "proton channels," has been receiving increasing attention from researchers in the field.[5–20] This singular kind of arrangements can be found for instance inside transmembrane proteins. In this case, an excess proton is "pumped" from one side of the membrane to the opposite, being then responsible for the generation of electrochemical potentials accross the membranes. Examples of this kind of proton transfer in biological systems are the F_0 component of ATP synthase;[21] the M2 proton channel of the A and B influenza viruses, which forms a proton channel necessary for the process of the uncoating of the virus;[22,23] the vacuolar H^+-ATPase (V-ATPase) and vacuolar H^+-pyrophosphatase (V-PPase), two proton-pump proteins crucial for the process of pH-homeostasis in endomembrane systems;[24] and the redox-driven proton pump in cytochrome *c* oxidase (C*c*O), a cornerstone of the energy transformation processes in biological systems.[25]

Transport of protons along a proton wire can also be initiated through photoactivation.[14,15,26–28] In this case, the trigger of the global proton traslocation is an excited-state proton transfer (ESPT): one of the transferable protons in the wire starts off bound to a photoactive molecule (chromophore). Absorption of a photon by the chromophore results in this case in increased acidity of the proton in the photoactive electronic excited state. The bond between chromophore and proton is much weakened, and proton transfer can take place. In some cases, the acidity of the proton in the photoactive state is so large that proton transfer in the excited state turns out to be barrierless, producing as a result ultrafast processes.[14,15,26–33] Given a proper arrangement of other proton acceptors and donors in the vicinity of the chromophore, proton transfer over large distances can occur also in an electronic excited state. Several cases of photoactivated proton-transfer processes involving a proton wire have been documented: the photocycle of retinal and bacteriorhodopsin[34] and the photocycle of the Green Fluorescent Protein (GFP)[35] and the asFP595 fluorescent protein.[36]

Because of the intrinsic interest of systems where multiple proton transfer occurs and the sometimes difficult interpretation of related experiments, detailed computational studies of these systems are necessary to lay the foundations of a sound understanding of their intricacies. After photoexcitation a series of ultrafast events may be triggered. They can be understood if a precise picture of the *real time* dynamics after photoexcitation (and therefore on one or several electronic excited-state PES) is available. Indeed, direct comparison of simulations to experimental measurements, e.g. pump−probe femtosecond spectra, is usually achieved via the computation of real-time correlation functions.[37] The inspection of the dynamics of the system after photoexcitation can also provide insightful mechanistical details just by following the evolution of classical trajectories or quantum wavepackets.

The problem of simulating such ultrafast processes can be conceptually divided in two major parts: 1) the computation of the underlying PES and 2) the solution of the dynamics of the nuclei on it. If classical dynamics, or more generally classical-trajectory based methods,[1,38] are to be used in the simulation, *ab initio* MD (AIMD)[39] methods may be employed with the features that the PES is only calculated there where it is needed and that they are full-dimensional in nature. These methods offer a convenient and combined solution to points 1) and 2). For ground electronic-state processes it is also possible to use polarizable force fields[40] or the empirical valence bond (EVB) method of Warshel[2,41] that accounts for bond forming and breaking at a much more reduced computational cost than AIMD methods. More recently another method has been proposed, which is suitable for condensed phase simulations and that combines Hartree−Fock molecular orbital (MO) and valence-bond (VB) theories to describe the PES of reactive systems (hence, MOVB method).[42–44]

It remains still the issue of whether classical-trajectory based methods can provide an accurate picture of the real-time dynamics following a photoexcitation event when light nuclei, e.g. protons, are involved.

Quantum dynamics is the correct theory to describe the motion of nuclei. However, converged quantum dynamics studies of large systems are nowadays not possible, and models of reduced dimensionality must be formulated when treating more than 6 or 7 atoms. The necessity to reduce the dimensionality of the problem arises basically from two factors. First, wavepacket methodologies based on grids require a global knowledge of the PES which must be computed on a grid of the order of 10^N points, where N is the dimensionality of the nuclear problem. Second, one must keep the problem of a size that is solvable by modern wavepacket methodologies such as the multiconfiguration time-dependent Hartree (MCTDH) method.[45] In this context, quantum dynamical, reduced-dimensionality investigations of processes involving the motion of light nuclei, such as proton-wires, appear as complementary and even necessary with respect to classical dynamics approaches. Reduced dimensionality studies of proton-transfer processes have been successfully carried on in the past on parametrized PESs and have the potential to unravel many important details of the systems under consideration.[46,47]

In this paper we present a convenient way to obtain a *parametrized* PES based on an affordable number of *ab initio* single-point calculations which is tailored to the simulation of proton-wires of the kind mostly found in biological systems, in which the proton-donor and proton-acceptor species in the wire can be rather heterogeneous. This covers our previous point 1) above. We formulate it bearing in mind that our goal is to perform quantum dynamics on the obtained PES, that is, our point 2). The PES we propose is part of a planar model of the proton-wire in which the proton positions and the donor−acceptor distances are the dynamical variables. The proposed PES and model are motivated by the fact that nowadays accurate quantum dynamical simulations are already feasible for 10 to 15 coupled degrees of freedom, which include many proton-wires within the range, while the computational cost of computing the full PES by DFT or *ab initio* methods for such systems is still far beyond reach. In a proton-wire with m transferable protons $2m$ bonds can be formed and broken. A PES able to describe such a

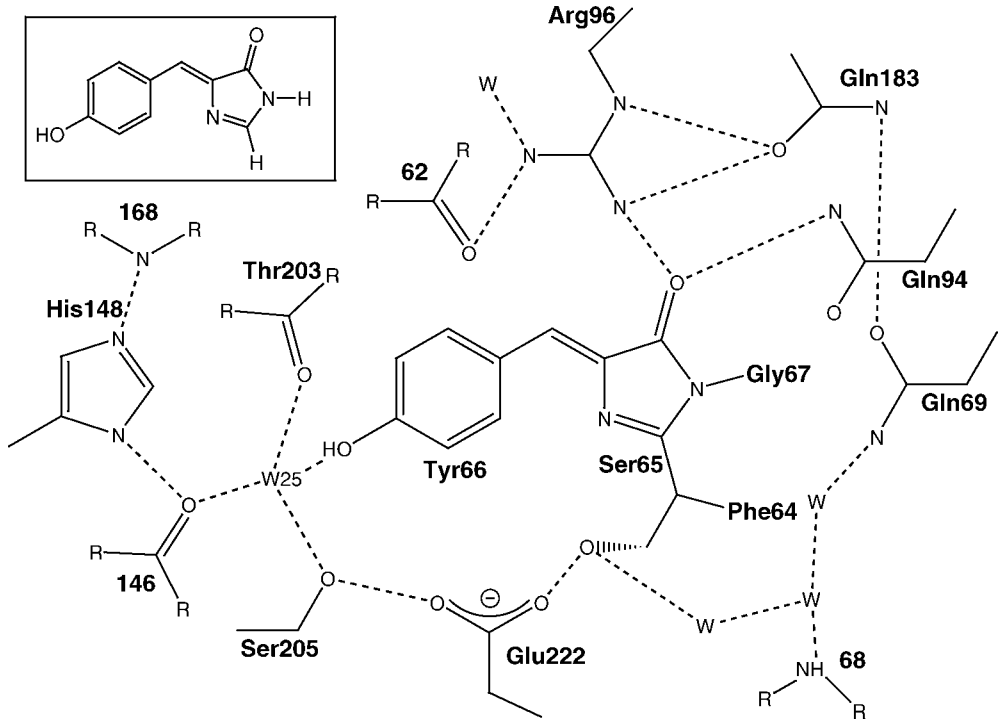

Figure 1. Schematic representation of the prevailing interactions surrounding the GFP chromophore. In the inset the isolated chromophore, *p*-hydroxybenzylideneimidazolinone, is shown.

system must then be able to describe bond breaking and forming correctly. To do so we base our approach on the EVB method[2,41] and present a convenient scheme to determine its parameters for the proton-wire at hand. It should be noted that a covalent bond or a hydrogen bond between a proton and a heavy atom in the wire will have different properties depending on the configuration of the rest of the wire. This could lead to an enormous number of parameters to describe all the different possibilities. The PES model is formulated such that the number of parameters involved keeps relatively low by exploiting the idea of protonation states. The number of *ab initio* reference points employed to fit the model PES is also kept as reduced as possible.

As an example of this computational approach the method will be applied to a system that has received much attention recently, the Green Fluorescent Protein (GFP) and its associated proton-wire.[35] GFP is a protein that occurs naturally in the North Pacific jellyfish *Aequorea Victoria* and that has found many uses as a biological fluorescent marker.[35] GFP absorbs in the blue region of the visible spectrum and has green fluorescence with a high quantum yield (0.72−0.85).[48–50] The structure of the protein has been described as a rigid cylinder made up of 11 β-sheets that shelter an α-helix supporting the chromophore roughly in the center of the cavity. The chromophore has been characterized as *p*-hydroxybenzylideneimidazolinone,[51,52] yet synthetic model compounds of the chromophore show no fluorescence,[53] indicating a strong influence of the microenvironment of the chromophore within the protein on the fluorescence. A detailed crystallographic description of GFP has been available for awhile[54] and has established that the chromophore is hydrogen-bonded to an internally caged water molecule (Wat25), which is bound to a serine residue (Ser205), which is finally bound to a glutamate residue (Glu222). While other interactions are present that help to stabilize the chromophore and keep it in place, there is nowadays consensus that the above-mentioned residues are the most relevant. See Figure 1 for a graphical description of these interactions. Wild-type GFP (wt-GFP) absorbs mainly at 397 nm, this having been identified with the absorption of the chromophore. The most widely accepted interpretation of the photophysical behavior of GFP is that photoexcitation of the chromophore triggers the operation of the proton-wire formed by the chromophore's phenolic group, Wat25, Ser205, and Glu222, including a total of three protons. The final product of this proton transfer, a protonated Glu222 residue, has been detected spectroscopically.[55,56] The green fluorescence emitted at 510 nm has been identified with the emission from the anionic (phenolate) form of the chromophore.[57] As described, the mechanism to induce fluorescence in GFP involves a heterogeneous proton-wire of three transferrable protons, with a total of four different chemical species supporting all the donor and acceptor atoms.

Our group has contributed to the theoretical knowledge on the dynamics of GFP previously. Static studies revealed that *in vacuo* the proton-transfer from the chromophore to the water molecule could occur involving a crossing of electronic states.[58] Later on, an extensive static study of the potential energy landscape controlling the triple proton-transfer in a model of the chromophore and intervening residues was undertaken.[18] This latter work is used in this paper to fit the potential energy surface functional form. The EVB approach described in the present work and in particular the PES obtained for the GFP proton-wire have been used recently to carry out a 6-dimensional quantum dynamical study of the proton-wire in GFP, in which the protein environment has not been included.[59] However, we note that, without loss of generality, the procedure described in this paper can be used to fit energy values coming from QM/MM methods.

The rest of this paper is organized as follows: section 2 discusses the theory, and in particular subsection 2.2 presents the methodological development of an EVB functional form for heterogeneous proton-wires; section 3 describes the application to the proton-wire in GFP; and finally section 4 concludes.

2. Theory

2.1. General EVB Potential. Each possible protonation state of the proton-wire is described by an EVB state. A protonation state is formally defined as a particular configuration of the hydrogen-bond system where each proton can formally be bonded to either the heavy atom at its left or at its right side. A proton-wire having m transferable protons is thus described, by $n = 2^m$ EVB states.

In the EVB theory the EVB states $|\phi_i\rangle$ appear only as a conceptual device, but they are neither directly calculated nor used. It is assumed that these states conform an orthonormal basis, $\langle\phi_i|\phi_j\rangle = \delta_{ij}$. The matrix elements of the EVB states $H_{ij} \equiv \langle\phi_i|\hat{H}|\phi_j\rangle$ are the actually relevant quantities, which are assumed to be functions of the positions of the nuclei, $H_{ij} \equiv H_{ij}(\mathbf{q})$. These matrix elements are typically described by parametrized functions similar to the usual molecular force fields. In practice, one constructs the EVB representation of the electronic Hamiltonian operator

$$\mathbf{H}(\mathbf{q}) = \begin{pmatrix} H_{11}(\mathbf{q}) & \cdots & H_{1n}(\mathbf{q}) \\ \vdots & & \vdots \\ H_{n1}(\mathbf{q}) & \cdots & H_{nn}(\mathbf{q}) \end{pmatrix} \tag{1}$$

and then diagonalizes it to get its eigenvalues and eigenvectors (From now on in the discussion, $\mathbf{q}$ may be sometimes dropped for the sake of clarity.). The only purpose of the EVB approach is to reproduce the PES of a particular electronic state (usually the ground electronic state, but not necessarily, as in this work) of a molecular system, with the extra property over traditional force fields that it is able to reproduce covalent bond breakage and formation. The PES of interest, representing the ground electronic state of the system or an excited electronic state, will be given invariably by the lowest eigenvalue of the $\mathbf{H}$ matrix, since the H_{ij} elements are parametrized for this purpose. It is important to stress at this point that the EVB form of the potential described above has nothing to do with the treatment of several electronic states of the molecular Hamiltonian in a diabatic or adiabatic representation. The approach is conceived to reproduce *only* a single PES as the lowest eigenvalue of the $\mathbf{H}$ matrix. We emphasize here that the use of an EVB-type PES to represent the potential of an excited electronic state is not new. It has been already used by some of us to describe an excited-state proton-transfer process in the condensed phase through a two-state EVB model.[33] More recent examples can also be found.[60] If the coupling between different electronic states were to come into play the present formulation should have to be modified.

The EVB PES is given by

$$V(\mathbf{q}) = \langle 0|\hat{H}|0\rangle \tag{2}$$

$$V(\mathbf{q}) = \sum_{i=1}^{n}\sum_{j=1}^{n} H_{ij} c_i^{(0)} c_j^{(0)} \tag{3}$$

which is equivalent to writing the eigenvalues equation for the EVB matrix

$$\mathbf{H}\,\mathbf{c}^{(0)} = E^{(0)}\,\mathbf{c}^{(0)} \tag{4}$$

where $\mathbf{c}^{(0)}$ is the eigenvector corresponding to the lowest eigenvalue, $E^{(0)} \equiv E^{(0)}(\mathbf{q}) \equiv V(\mathbf{q})$ and $|0\rangle \equiv \mathbf{c}^{(0)}$.

2.2. EVB Matrix-Elements for an Heterogeneous Proton-Wire. *2.2.1. Diagonal Elements.* The diagonal element H_{ii} describes the potential of the EVB state i which, as mentioned above, corresponds to a particular protonation state of the wire. In a wire of m protons there are m covalent bonds per protonation state that will be described by some sort of function. In addition we include functions that take into account nonbonded van der Waals interactions. The diagonal term describing the ith protonation state is given in general by

$$H_{ii} = \sum [\text{bond. interac.}] + \sum [\text{nonbond. interac.}] + \Delta_i + \Delta_{tot} \tag{5}$$

The different terms appearing in the diagonal of the EVB matrix are discussed in what follows.

Bonding Interactions. A possible strategy is to consider each bond in each protonation state as different, which means described by a different parametrized function. In a wire with m transferable protons the number of protonation (EVB) states is given by $n = 2^m$. For each protonation state one must specify m bonding interactions, one for each proton, leading to a total of $m \times 2^m$ functions to describe bonding interactions. The number of bonding interactions to be parametrized grows exponentially under such scheme. The exponential growth may be cut down to linear by assuming that each heavy atom in the wire is able to form two types of bonds with the transferring protons: For a given protonation state a nonterminal residue can have 0, 1, or 2 protons attached. In the first case that residue holds a hole of the wire and a formal negative charge. In the last case it holds the extra proton and a formal positive charge. Only when a residue has 1 or 2 protons attached can a covalent bond be conceived, being the bond, in principle, of a different nature in each case. Thus, for every different nonterminal residue two new types of covalent bonds are taken into account. Using a similar argument the terminal residues add a new type of bond each. Adopting this model for the bonding interactions, it is easy to see that a proton-wire with m transferable protons, where all the residues are different, has a total number of $2m$ bond types. The other limiting case, a system where all the residues are of the same kind (e.g., water), could be described by *only* 2 different bond types.[61]

Morse potentials are usually employed for the bonding interactions when constructing EVB potentials

$$M(d) = D[1 - e^{-\beta(d-d^0)}]^2 \tag{6}$$

where d is the distance from the proton to the heavy atom.

Besides, bond-angle and torsional deformations are also counted among the bonding interactions. Usually, the bond-angle deformations are described using a harmonic-like potential term

$$A(\theta) = \frac{1}{2}k_\theta(\theta - \theta^0)^2 \quad (7)$$

where θ would be the angle formed by three consecutive atoms in the wire. As for torsional contributions to bonding interactions, they are usually parametrized with terms of the form

$$D(\varphi) = k_\varphi[1 + \cos(n\varphi - \varphi^0)] \quad (8)$$

where n represents the periodicity of the torsional potential.

Nonbonding Interactions. For the nonbonding interactions, Coulomb and/or van der Waals interactions can be considered. In the case of the Coulomb interactions, a charge is assigned to each atom in every protonation state, and the charges are adjusted along with the rest of parameters

$$E = \sum \frac{1}{4\pi\varepsilon_0\varepsilon_r}\frac{q_i q_j}{r_{ij}} \quad (9)$$

where the summation runs over all nonbonded atom pairs.

van der Waals interactions are important to maintain the structure of the wire and to represent the nonbonding interactions of the protons and heavy atoms, namely the hydrogen bonds. van der Waals interactions between protons and heavy atoms to which they are not bonded force the potential energy to increase when a proton tries to enter the vicinity of this heavy atom to which it is not bonded. Interactions between heavy atoms keep them from flying apart and control the donor−acceptor distance which is important to have well-described hydrogen bonds. The model of nonbonding interactions is as follows: a proton has a nonbonding interaction with a neighbor heavy atom if this proton has no covalent bond with it. The type of the nonbonding interaction is independent of the configuration of the rest of protons in the wire and depends only on the type of the residue. In a chain with m protons this gives rise to $2m$ different van der Waals interactions, two for each proton, one with each different neighbor. The interaction of a pair of adjacent heavy atoms gives rise to a particular van der Waals type, independent of the protonation state of the system. In a chain of m protons this results in m different van der Waals interactions between the heavy atoms. The 12−6 van der Waals function has been adopted to describe the nonbonding interactions

$$W(d) = 4\varepsilon[(\frac{\sigma}{d})^{12} - (\frac{\sigma}{d})^6] \quad (10)$$

Shifts. Each EVB state is added a shift term Δ_i. This term is meant to give flexibility to the EVB states so that the relative energies between them can adjust without placing strain on the parameters of the bonding and nonbonding interactions. Moreover, adding or subtracting the same constant k to all Δ_i values shifts the whole potential by k. It is important that all Δ_i's can vary independently since this degree of freedom allows the potential as a whole to approach the reference energies without changing its shape. In the event that the *shape* of the potential would be good but its absolute values be shifted by some amount k from the reference energies, a simple shift in all Δ_i's by an amount k would suffice to improve the overall fit. Instead of allowing all Δ_i's to change independently, one of them is always kept fixed at 0, so that the $(n-1)$ Δ_i values turn into relative shifts with respect to the fixed one. The degree of freedom that has been lost in parameter space is recovered by introducing a total shift, Δ_{tot}. By introducing a single parameter that controls the total shift the fitting procedure becomes more stable.

2.2.2. Coupling Terms. The EVB coupling terms are the nondiagonal elements of the EVB matrix. If the EVB matrix is taken to be real and symmetric, the number of different coupling terms is $n(n-1)/2$, n being the number of EVB states. Using again the relation between n and the number of transferrable protons m, the number of coupling terms is given by $2^{2m-1}-2^{m-1}$, again an exponential growth with the number of transferrable protons. In order to avoid the inclusion of so many coupling terms, and hence of many parameters into the functional form of the PES being adjusted, only the coupling terms between protonation states interconvertible by transfer of *a single proton* are considered. Such assumption in the functional form does not represent a problem in the description of concerted proton motions: If data points are included belonging to such regions of configurational space, the functional form as a whole will adjust to represent them correctly as the full set of parameters is optimized. Within this model the number of coupling terms is cut down to $m2^{m-1}$, which is however still exponential but with a much smaller growth rate. This scheme also facilitates the consideration of wires where all the residues are equal, since a single type of coupling needs to be considered: that corresponding to the transfer of a proton from a residue to another (which still appears in $m \times 2^{m-1}$ positions at each side of the diagonal in the EVB matrix).

The coupling terms can be treated in different ways. One possibility is to use Gaussian functions. This approach has the advantage that far from the strong interaction region the coupling vanishes smoothly and the equilibrium regions are cleanly described by one single EVB state. Thus, the EVB diagonal terms can be general force fields that were previously parametrized and are not being refitted. The couplings take care only of the interaction region. This is not our case, since we fit all the parameters simultaneously with respect to a set of reference *ab initio* energies. In such a case constant coupling terms for each electronic state are justified, which add a single parameter each to the functional form and facilitate the fitting. Using constant couplings with general force fields may destroy the properties of the force field in the noninteracting regions, but again this is not the case here, since we are only interested in having a global potential, flexible enough and yet tailored to reproduce a proton-wire potential after determination of its parameters.

3. Application to the GFP Proton-Wire

3.1. Specification of the EVB Matrix Elements. The proton-wire in GFP includes three transferrable protons. Hence, there are $2^3 = 8$ possible protonation states. This leads to a real symmetric 8-states EVB matrix:

Table 1. Equivalence between EVB States—Diagonal Elements in the EVB Matrix, Eq *11*—and Protonation States, Here Given as a 3-Digit Binary Number[a]

EVB state	protonation state	
	this work	refs 18 and 59
1	000	CWS
2	100	WWS
3	010	CSS
4	001	CWG
5	110	WSS
6	101	WWG
7	011	CSG
8	111	WSG

[a] See the main text for details. In the third column, the denomination of each protonation state is also given as in our related work in GFP in refs 18 and 59: each protonation state of the wire is referenced by a three-letter code where the first, second, and third letter identify the heavy atom supporting the first, second, and third proton of the wire, respectively, following this key: *C*: chromophore, *W*: Wat25, *S*: Ser205, and *G*: Glu222.

$$\mathbf{H}(\mathbf{q}) = \begin{pmatrix} H_{11} & H_{12} & H_{13} & H_{14} & 0 & 0 & 0 & 0 \\ H_{12} & H_{22} & 0 & 0 & H_{25} & H_{26} & 0 & 0 \\ H_{13} & 0 & H_{33} & 0 & H_{35} & 0 & H_{37} & 0 \\ H_{14} & 0 & 0 & H_{44} & 0 & H_{46} & H_{47} & 0 \\ 0 & H_{25} & H_{35} & 0 & H_{55} & 0 & 0 & H_{58} \\ 0 & H_{26} & 0 & H_{46} & 0 & H_{66} & 0 & H_{68} \\ 0 & 0 & H_{37} & H_{47} & 0 & 0 & H_{77} & H_{78} \\ 0 & 0 & 0 & 0 & H_{58} & H_{68} & H_{78} & H_{88} \end{pmatrix} \quad (11)$$

Table 1 indexes each diagonal term in the EVB matrix in eq 10 with the corresponding protonation state of the GFP proton-wire. In order to label in a systematic way the protonation states in GFP, we propose a naming scheme that is concise and can easily be extended to represent any conceivable linear proton wire. The labeling scheme plays with the idea of protonation states, a protonation state being a structure in which each proton is within bonding distance to either its donor or acceptor atom. The protonation state is represented by a binary number with 3 digits, each of them assigned, respectively, to the Cro-Wat25, Wat25-Ser205, and Ser205-Glu222 hydrogen bond. In case that one of the three protons is in bonding distance to its donor atom it is represented by "0". If the proton is within bonding distance to the acceptor atom it is represented by "1". Since there are three transferable protons, the protonation states can be referred to as a binary number of three digits with a total of $2^3 = 8$ protonation states. The idea of protonation states we are using does not assume anything about their stability; it is simply a convenient way of referring to the different structures relevant to the proton-wire. Using such convention, reactants are represented by (000), products are represented by (111), the situation in which only the proton shared by the chromophore and Wat25 has transferred would be given by (100), and so on. This naming scheme can straightforwardly be generalized to a proton-wire of m protons, by using an m-digit binary number to represent the 2^m protonation states.

Even though all elements in the matrix in eq 11 could be functions of all coordinates $\mathbf{q}$, a different choice has been adopted here. As explained in the previous section, the nondiagonal terms in eq 11 are just parameters (that is, not functions of the coordinates $\mathbf{q}$). The diagonal terms are functions of the coordinates and are given by

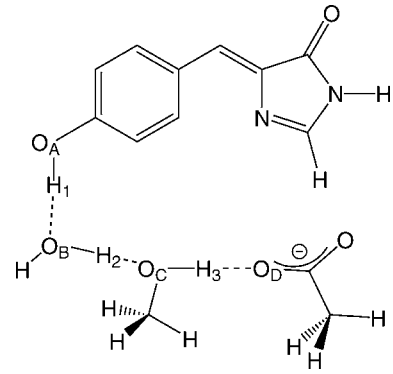

Figure 2. Chemical model used in ref 18 and in this work to compute the potential energies of selected structures used in the fit.

$$H_{ii} = B_i + W_i + W_{\text{chain}} + \Delta_i + \Delta_{tot} \quad (12)$$

where B_i is the bonding contribution of the protonation state i, W_i is the nonbonding contribution between protons and oxygens forming hydrogen bonds in the ith protonation state, and W_{chain} are the nonbonding contributions between neighboring oxygen atoms, which are the same in each protonation state. Δ_i is the state-specific energy-shift parameter and Δ_{tot} is the total shift parameter.

In a previous work in which a lengthy molecular-dynamics simulation of GFP was performed, we showed that the proton-wire was well formed over time and that it remained approximately planar.[18] Thus, it seems reasonable to drop from the bonding interactions those that imply departure from planarity or torsional potential energy terms. Furthermore, as will be explained soon, the reference data against which the EVB functional form will be fitted will come from a reduced model of the proton-wire, used before in our previous study[18] and represented here in Figure 2. In this model, the effect of the rigid stucture of the protein surrounding the proton-wire is not accounted for, and, thus, terms of bond-angle deformation of the heavy atoms (i.e., depending on $O_AO_BO_C$ or $O_BO_CO_D$—see Figure 2) cannot be meaningfully included in the bonding interactions, because the rigid structure of the cavity where the proton-wire lies is missing in the reduced model. For this study, we choose as bonding contributions those that come directly from the stretching of the bonds between the protons and the donor and acceptor atoms. Within this approach, the seven atoms forming the wire being restricted to lie in a plane require $2 \times 7 = 14$ degrees of freedom, from which only 11 correspond to internal motion (2 for the center of mass on the plane and one for in-plane rotation). If the bending motion of the heavy atoms is not allowed, the number of degrees of freedom remaining is $11 - 2 = 9$.

The bonding contributions are then given by

$$\begin{aligned} B_1 &= M_A(d_{A1}) + M_{B-}(d_{B2}) + M_{C-}(d_{C3}) \\ B_2 &= M_{B+}(d_{1B}) + M_{B+}(d_{B2}) + M_{C-}(d_{C3}) \\ B_3 &= M_A(d_{A1}) + M_{C+}(d_{2C}) + M_{C+}(d_{C3}) \\ B_4 &= M_A(d_{A1}) + M_{B-}(d_{B2}) + M_D(d_{3D}) \\ B_5 &= M_{B-}(d_{1B}) + M_{C+}(d_{2C}) + M_{C+}(d_{C3}) \\ B_6 &= M_{B+}(d_{1B}) + M_{B+}(d_{B2}) + M_D(d_{3D}) \\ B_7 &= M_A(d_{A1}) + M_{C-}(d_{2C}) + M_D(d_{3D}) \\ B_8 &= M_{B-}(d_{1B}) + M_{C-}(d_{2C}) + M_D(d_{3D}) \end{aligned} \quad (13)$$

with

$$M_{X*}(d_{Xn}) = D_{X*}[1 - e^{-\beta_{X*}(d_{Xn} - d^0_{X*})}]^2 \quad (14)$$

where d_{Xn} (and d_{nX}) is the distance between oxygen X and proton n (with A being the phenolic oxygen in Cro, B the oxygen in Wat25, C the oxygen in Ser205, and D the acceptor oxygen in Glu222; proton 1 is shared between Cro-Wat25, proton 2 between Wat25-Ser205, and proton 3 between Ser205-Glu222: see Figure 2), D_{X*}, β_{X*}, and d^0_{X*} are parameters, and $*$ may be $+$, $-$, or blank: $+$ and $-$ refer to the Morse potentials of the nonterminal residues supporting 2 and 1 protons, respectively, and a blank refers to the Morse potential for terminal residues supporting a proton.

Let us consider the nonbonding contributions. In our case, the consideration of electrostatic terms (i.e., charges) was found to be redundant with the bonding interactions and not necessary to describe the proton-wire, since each atom moves in a relatively small region of configurational space. It has to be recalled that the final goal is to achieve a good description of the PES by fitting the EVB potential to some reference data, and the inclusion of charges led in this case to an overparametrization of the model. As a consequence, the only terms actually considered in the nonbonding contributions are van der Waals terms. Within these considerations, the nonbonding contributions of each O—H hydrogen bond are given by

$$\begin{aligned} W_1 &= W_{1B}(d_{1B}) + W_{2C}(d_{2C}) + W_{3D}(d_{3D}) \\ W_2 &= W_{A1}(d_{A1}) + W_{2C}(d_{2C}) + W_{3D}(d_{3D}) \\ W_3 &= W_{1B}(d_{1B}) + W_{B2}(d_{B2}) + W_{3D}(d_{3D}) \\ W_4 &= W_{1B}(d_{1B}) + W_{2C}(d_{2C}) + W_{C3}(d_{C3}) \\ W_5 &= W_{A1}(d_{A1}) + W_{B2}(d_{B2}) + W_{3D}(d_{3D}) \\ W_6 &= W_{A1}(d_{A1}) + W_{2C}(d_{2C}) + W_{C3}(d_{C3}) \\ W_7 &= W_{1B}(d_{1B}) + W_{B2}(d_{B2}) + W_{C3}(d_{C3}) \\ W_8 &= W_{A1}(d_{A1}) + W_{B2}(d_{B2}) + W_{C3}(d_{C3}) \end{aligned} \quad (15)$$

The O—O nonbonding contributions are equal for all protonation states and are given by

$$W_{\text{chain}} = W_{AB}(d_{AB}) + W_{BC}(d_{BC}) + W_{CD}(d_{CD}) \quad (16)$$

where d_{XY} is the distance between oxygen atoms X and Y. The 6−12 van der Waals terms have been adopted for the nonbonding interactions

$$W_{XY}(d_{XY}) = 4\varepsilon_{XY}[(\frac{\sigma_{XY}}{d_{XY}})^{12} - (\frac{\sigma_{XY}}{d_{XY}})^{6}] \quad (17)$$

Globally the potential energy surface is obtained as the lowest eigenvalue of the matrix in eq 11 and depends on a total of 9 independent variables: the distances between each donor and acceptor oxygen atom (d_{AB}, d_{BC}, d_{CD}), the distances between donor atom and the transferring proton (d_{A1}, d_{B2}, d_{C3}), and the distances between acceptor atom and the transferring proton (d_{1B}, d_{2C}, d_{3D}):

$$V = V(d_{AB}, d_{BC}, d_{CD}, d_{A1}, d_{B2}, d_{C3}, d_{1B}, d_{2C}, d_{3D}) \quad (18)$$

This model as it stands is valid for a system where all proton-wire atoms are contained in the same plane and where bending of the heavy atoms is not allowed.

3.2. Fitting of the EVB Functional Form. To save computational effort each of the three hydrogen bonds in GFP has been kept linear (that is, the proton moves in a straight line from donor to acceptor atom). Because in the model each hydrogen bond is now restricted to remain linear, distances between donor and acceptor, proton and acceptor, and proton and donor of each hydrogen bond are related:

$$\begin{aligned} d_{AB} &= d_{A1} + d_{1B} \\ d_{BC} &= d_{B2} + d_{2C} \\ d_{CD} &= d_{C3} + d_{3D} \end{aligned} \quad (19)$$

This reduces effectively the number of degrees of freedom of the system to 6.

The reference data points used to adjust the parameters of the PES have been partially published in a related work.[18] A brief summary of the level of calculation and strategy followed is given here: The potential energy was evaluated for both the S_0 and S_1 states at the CASPT2 level with an active space of six electrons in six π molecular orbitals on 252 different geometries of the chain.[18] The system was modeled to reduce the number of atoms involved and is depicted in Figure 2.

The chemical modelization included forced planarity of the system and substitution of the Ser205 residue by a methanol and of the Glu222 residue by an acetate. The restriction of planarity was justified by the results of a long-time molecular dynamics simulation of the ground state.[18] The geometries were generated along each possible path involving a single proton transfer event (giving a total of 12 paths: see Figure 3) and for three different oxygen—oxygen distances in each case. Seven equidistant positions of the transferring proton were scanned for each path and each donor—acceptor distance. As for the rest of the atoms in the model, their relative positions were held fixed at their values in the minimum in the ground electronic state, S_0. When oxygen atoms were displaced along the wire (change of a d_{XY} coordinate) the potential energy was computed for a structure where the distance between the oxygen atoms and their supporting residues was kept fixed (that is, the residues were translated alongside with the oxygen atom with fixed relative coordinates). Using this procedure, the potential energies of the ground electronic state and the photoactive $\pi\pi^*$ state have been obtained. To this large number of single-point calculations an extra set of 86 additional points has been calculated to improve the description of some areas of configurational space that were not relevant for a static study (such as that carried out in ref 18) but that have a certain effect in the asymptotic regions of the potential energy function that is fitted in this work, which become relevant in dynamical studies, where high-energy regions can support

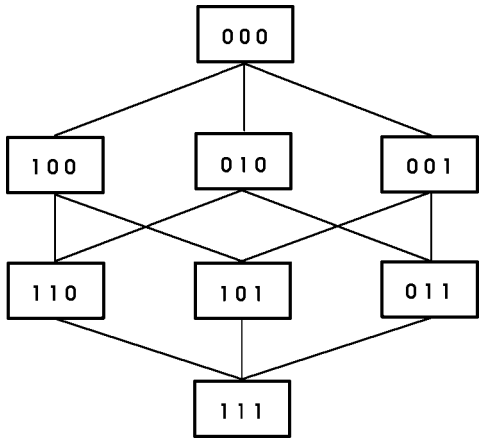

Figure 3. Schematic representation of the different paths connecting the eight possible protonation states of the proton-wire.

a certain amount of density over time.[59] Besides, we have added structures where all protons are exactly in the middle of their respective hydrogen bonds, and structures where two given protons are exactly in the middle of their respective hydrogen bonds, while the third is bound to either the donor or the acceptor atom. These structures are important to describe the three possible concerted double proton transfers and the also possible concerted triple proton transfer. Details on the structures and energetics of this extra set are included in the Supporting Information. Overall, the total number of reference data point against which the potential energy functions have been fitted amounts to 338.

Next, the error function

$$E(\mathbf{p}) = \sqrt{\frac{\sum_i^{N_p} w_i (V(\mathbf{q}_i;\mathbf{p}) - V_{ref}(\mathbf{q}_i))^2}{N_p}} \qquad (20)$$

which depends solely on the set of parameters **p**, is minimized using a simplex minimization algorithm.[62] The EVB functional form of each surface depends on a total of 56 adjustable parameters. N_p is the number of configurations for which a reference energy is known (338 in our case). w_i is a weight function that is introduced in order to favor the fit in regions of low potential energy with respect to high energy less relevant regions. The weight is defined as follows

$$w_i \equiv w(v_i) = \begin{cases} 1 & \text{if } v_i \le v_c \\ e^{-(v_i - v_c)/\alpha} & \text{if } v_i > v_c \end{cases} \qquad (21)$$

where v_i is the *ab initio* potential energy value at point q_i, v_c is a cutoff potential that controls the domain of action of the weight, and α controls the rate at which the weight goes to 0 as the energy increases. At this point we highlight that of all the energy shifts Δ_i, one is taken as fixed in our model per each electronic state. For the PES of S_0, Δ_1 has been held fixed at 0, because this corresponds to the 000 (CWS) protonation state of S_0, known to be the most stable. Likewise, in S_1 it is Δ_8 that has been held fixed at 0, since it corresponds to the 111 (WSG) species, which has been described as the most stable protonation state in S_1.[18]

The fit was carried out for S_0 and S_1. In both cases, v_c was made equal to the lowest energy of the *ab initio* reference data for the corresponding electronic state *plus* 15 kcal mol^{-1}, and α = 10 kcal mol^{-1}. The optimization procedure was carried out until E in eq 20 was minimized. The parameters obtained are collected in Tables 2 for S_0 and 3 for S_1.

Table 2. Parameters of the Potential Energy Surface for the Ground State S_0

parameter	value	units	parameter	value	units
D_A	141.38	kcal/mol	σ_{C3}	1.36	Å
β_A	2.024	Å^{-1}	ε_{AB}	8.48	kcal/mol
d^0_A	0.98	Å	σ_{AB}	2.34	Å
D_{B-}	81.30	kcal/mol	ε_{BC}	4.32	kcal/mol
β_{B-}	2.51	Å^{-1}	σ_{BC}	2.40	Å
d^0_{B-}	0.98	Å	ε_{CD}	0.90	kcal/mol
D_{B+}	114.33	kcal/mol	σ_{CD}	2.67	Å
β_{B+}	1.88	Å^{-1}			
d^0_{B+}	1.010	Å	H_{12}	17.69	kcal/mol
D_{C-}	188.22	kcal/mol	H_{13}	33.62	kcal/mol
β_{C-}	1.52	Å^{-1}	H_{14}	58.03	kcal/mol
d^0_{C-}	0.95	Å	H_{25}	79.41	kcal/mol
D_{C+}	155.32	kcal/mol	H_{26}	20.90	kcal/mol
β_{C+}	1.27	Å^{-1}	H_{35}	90.92	kcal/mol
d^0_{C+}	0.34	Å	H_{37}	52.75	kcal/mol
D_D	414.44	kcal/mol	H_{46}	45.18	kcal/mol
β_D	0.79	Å^{-1}	H_{47}	48.02	kcal/mol
d^0_D	0.81	Å	H_{58}	99.85	kcal/mol
ε_{1B}	0.0032	kcal/mol	H_{68}	18.94	kcal/mol
σ_{1B}	1.58	Å	H_{78}	29.33	kcal/mol
ε_{2C}	4.41	kcal/mol	Δ_1	0 (fixed)	kcal/mol
σ_{2C}	1.01	Å	Δ_2	78.48	kcal/mol
ε_{3D}	1.22	kcal/mol	Δ_3	10.54	kcal/mol
σ_{3D}	1.09	Å	Δ_4	62.03	kcal/mol
ε_{A1}	−0.0016	kcal/mol	Δ_5	87.63	kcal/mol
σ_{A1}	1.18	Å	Δ_6	41.65	kcal/mol
ε_{B2}	0.0828	kcal/mol	Δ_7	40.84	kcal/mol
σ_{B2}	1.21	Å	Δ_8	50.02	kcal/mol
ε_{C3}	0.0859	kcal/mol	Δ_{tot}	44.18	kcal/mol

Table 3. Parameters of the Potential Energy Surface for the Photoactive Excited State S_1

parameter	value	units	parameter	value	units
D_A	232.20	kcal/mol	σ_{C3}	1.09	Å
β_A	1.31	Å^{-1}	ε_{AB}	1.35	kcal/mol
d^0_A	0.87	Å	σ_{AB}	2.58	Å
D_{B-}	65.32	kcal/mol	ε_{BC}	1.93	kcal/mol
β_{B-}	2.54	Å^{-1}	σ_{BC}	2.48	Å
d^0_{B-}	0.99	Å	ε_{CD}	1.43	kcal/mol
D_{B+}	287.23	kcal/mol	σ_{CD}	2.54	Å
β_{B+}	1.38	Å^{-1}			
d^0_{B+}	−0.28	Å	H_{12}	142.19	kcal/mol
D_{C-}	113.46	kcal/mol	H_{13}	18.36	kcal/mol
β_{C-}	2.32	Å^{-1}	H_{14}	3.56	kcal/mol
d^0_{C-}	0.98	Å	H_{25}	193.63	kcal/mol
D_{C+}	53.00	kcal/mol	H_{26}	−123.23	kcal/mol
β_{C+}	1.35	Å^{-1}	H_{35}	70.47	kcal/mol
d^0_{C+}	0.86	Å	H_{37}	92.51	kcal/mol
D_D	169.94	kcal/mol	H_{46}	168.46	kcal/mol
β_D	1.53	Å^{-1}	H_{47}	−37.96	kcal/mol
d^0_D	0.88	Å	H_{58}	104.49	kcal/mol
ε_{1B}	0.20	kcal/mol	H_{68}	2.50	kcal/mol
σ_{1B}	1.38	Å	H_{78}	37.68	kcal/mol
ε_{2C}	0.94	kcal/mol	Δ_1	24.87	kcal/mol
σ_{2C}	−1.03	Å	Δ_2	−39.74	kcal/mol
ε_{3D}	0.26	kcal/mol	Δ_3	140.00	kcal/mol
σ_{3D}	1.22	Å	Δ_4	95.67	kcal/mol
ε_{A1}	5.75	kcal/mol	Δ_5	−10.03	kcal/mol
σ_{A1}	0.96	Å	Δ_6	−213.73	kcal/mol
ε_{B2}	0.39	kcal/mol	Δ_7	59.10	kcal/mol
σ_{B2}	−1.18	Å	Δ_8	0 (fixed)	kcal/mol
ε_{C3}	0.56	kcal/mol	Δ_{tot}	147.75	kcal/mol

Table 4. Energy-Dependent RMS of the Fitted Potential with Respect to the Reference *ab Initio* Points, for the Ground State S_0[a]

E_{lim}	RMS	N
10.0	0.946	30
20.0	1.390	96
30.0	1.575	175
40.0	1.737	238
50.0	1.933	292
60.0	2.483	319
70.0	2.839	336
80.0	2.836	338

[a] The RMS (second column, in kcal mol^{-1}) has been computed for all reference structures whose energy is within E_{lim} (first column, in kcal mol^{-1}) of that of the lowest-energy structure in S_0. *N* indicates how many structures meet the energy criterion.

Table 5. Energy-Dependent RMS of the Fitted Potential with Respect to the Reference *ab Initio* Points, for the Photoactive State S_1[a]

E_{lim}	RMS	N
80.0	1.325	10
90.0	1.397	75
100.0	1.503	201
110.0	1.841	261
120.0	2.522	305
130.0	3.458	332
140.0	3.672	338

[a] The RMS (second column, in kcal mol^{-1}) has been computed for all reference structures whose energy is within E_{lim} (first column, in kcal mol^{-1}) of that of the lowest-energy structure in S_0. *N* indicates how many structures meet the energy criterion.

Ever since the weights are introduced in the error function its value does not have the same direct meaning as an RMS, for instance. To assess the goodness of the fit, instead, a set of energy-dependent RMS of the fit with respect to the *ab initio* data has been computed and is shown in Tables 4 (S_0) and 5 (S_1). In this way, it is possible to appreciate that an acceptable RMS under 1.6 kcal mol^{-1} is achieved, for instance, for energies within 30 kcal mol^{-1} of the minimum in the ground state S_0 (comprising 175 structures). A comparable rms of 1.5 kcal mol^{-1} is achieved for up to 201 structures that are within 100 kcal mol^{-1} of the S_0 minimum, this time for the photoactive state S_1. Taking into account the inherent complexity of potential-fitting, we think that the fittings for S_0 and S_1 are satisfactory and thus that the potential energy functions obtained correctly and almost quantitatively describe the CASPT2 energetics of the low-lying areas of both the ground and photoactive states of the model system in Figure 2.

Figures 4 and 5 display the deviations from the fitted values with respect to the reference points. It can be seen that for both electronic states the fitted values agree within chemical accuracy (~1 kcal mol^{-1}) with reference data for structures within 10−20 kcal mol^{-1} of the lowest *ab initio* energy for that state. Agreement for the rest of the surface is good, as the RMS values indicate. The quality of the fitted energies decreases as absolute energy increases. This is due to the effect of the weights in the error function, which are introduced to allow a smoother fit for the relevant (i.e., low-energy) areas of each potential energy surface.

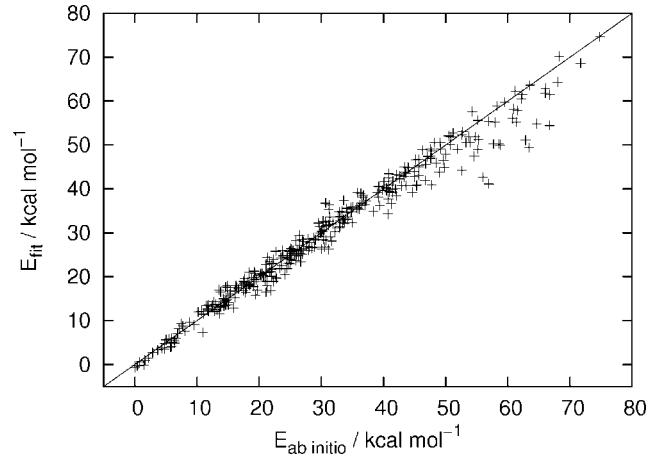

Figure 4. Deviation of the fitted values with respect to the *ab initio* reference points for the ground state S_0. Points on the diagonal are perfectly fitted to the *ab initio* reference data.

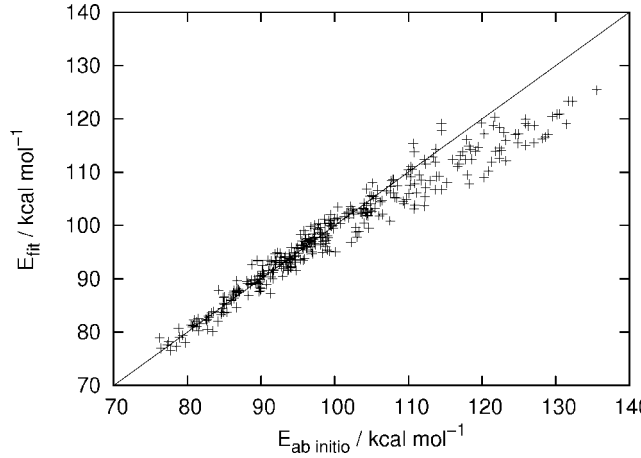

Figure 5. Deviation of the fitted values with respect to the *ab initio* reference points for the photoactive state S_1. Points on the diagonal are perfectly fitted to the *ab initio* reference data.

3.3. Analysis of the Fitted Potential Energy Surfaces. The availability of the 6-dimensional fitted surfaces for S_0 and S_1 makes an exhaustive exploration of the energetics of the wire feasible, such that the results would be, in quality terms, equivalent to an exploration of the chemical model (Figure 2) but avoiding the expensive optimizations involved. Besides, as will be discussed below, some of the energetic terms —specifically those including nuclear dynamic corrections—can only be computed from this model.

3.3.1. Static Analysis: Stationary Points. Even though a total of 8 protonation states can be thought of, it is not clear whether all of them exist as chemical entities or whether the same exist both in S_0 and S_1. An exhaustive search for the points with a null potential energy gradient has been undertaken. Figure 6 shows the energy of such points, and Figure 7 summarizes the geometry of the proton-wire for each of these stationary points.

S_0 has only one minimum where the reactants region is (000, or CWS structure). All attempts to locate other minima

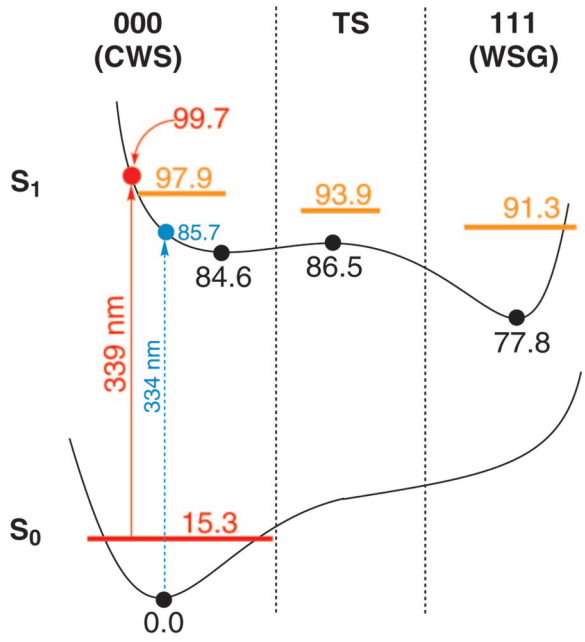

Figure 6. Schematic representation of the energetics of the operation of the proton-wire in GFP. The legend at the heading indicates the 'chemical' name of the different regions on the potential energy surface (PES). Black circles identify a stationary point, and figures in black denote the *Born−Oppenheimer potential energy* values of stationary points on the S_0 and S_1 PESs. The light blue arrow and the corresponding circle indicate the Franck−Condon transition without considering kinetic energy. The red arrow and corresponding circle indicate the Franck−Condon transition including kinetic energy. Horizontal segments identify the zero-point energy level of chemical species. Figures (and likewise, segments) in red represent exact values—within the model—for total energy obtained through dynamical simulations, while figures in orange represent estimated values for the total energy obtained assuming harmonic vibrations. All units, except where explicitly indicated, are kcal mol^{-1}.

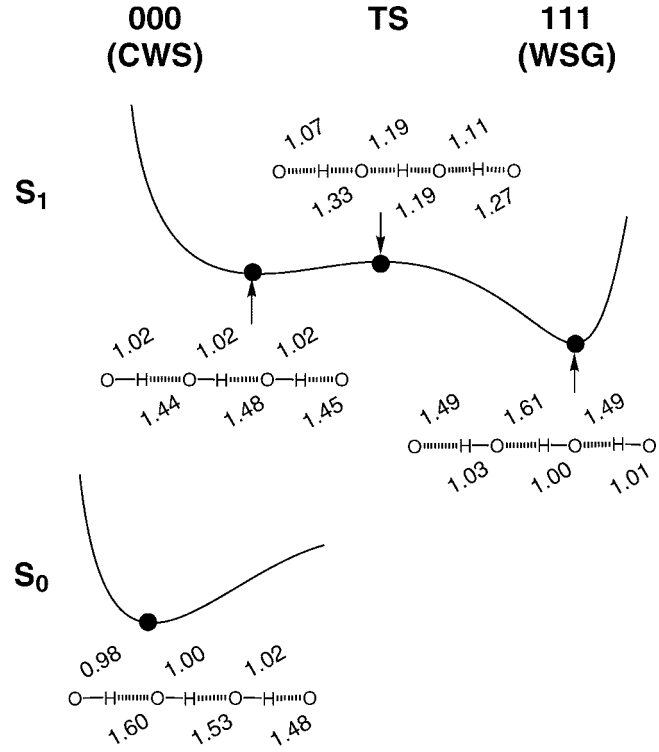

Figure 7. Schematic representation of the geometry of the proton-wire in the model in the stationary points found (solid circles) on the fitted potential energy surface.

corresponding to the remaining protonation states led invariably to this structure. In S_1 a total of two different minima have been found: the first corresponds to the reactants' structure (000, or CWS), +84.6 kcal mol^{-1} above the minimum in S_0, while the second corresponds to the final product of the wire (111, or WSG), +77.8 kcal mol^{-1} above the minimum in S_0 or 6.8 kcal mol^{-1} below the reactants' structure in S_1. Hence, the 000 → 111 process in S_1 is exoergic. The transition state structure connecting both minima has been found to be only +1.9 kcal mol^{-1} above the reactants' in S_1.

The structural changes brought up by photoexcitation are shown in Figure 7. Upon excitation, the three hydrogen bonds are shortened noticeably: Cro-Wat25 goes from 2.58 Å to 2.46 Å ($\Delta d_{AB} = -0.12$), Wat25-Ser205 from 2.53 Å to 2.50 Å ($\Delta d_{BC} = -0.03$), and Ser205-Glu222 from 2.50 Å to 2.47 Å ($\Delta d_{CD} = -0.03$). This goes in line with the elongation of the donor-proton distance, which is +0.04 Å for the chromophoric proton (Δd_{A1}) and +0.02 Å for the Wat25 proton (Δd_{B2}) and no appreciable change for the Ser205 proton (Δd_{C3}). This behavior is reasonable: accepting that photoexcitation is localized on the chromophore, the further away from Cro the proton is, the smaller the distortion of the donor−H bond is. In terms of proton motion, it seems that the chromophoric proton moves further when comparing the S_0 and S_1 000 (CWS) structures. The transition state structure for the 000 → 111 process in S_1 represents approximately a concerted process, although asynchronous. To measure the degree of asynchronicity, we define the position asymmetry coordinate δ_i as follows ($i = 1$ for the Cro-Wat25, 2 for Wat25-Ser205, and 3 for Ser205-Glu222 hydrogen bond, respectively):

$$\begin{aligned} \delta_1 &= d_{A1} - d_{1B} \\ \delta_2 &= d_{B2} - d_{2C} \\ \delta_3 &= d_{C3} - d_{3D} \end{aligned} \tag{22}$$

When $\delta_i = 0$ this indicates that the ith proton is exactly in the middle of the hydrogen bond, or, in other words, its transfer is 50% complete. The values determined for the transition state structure are $\delta_1 = -0.26$, $\delta_2 = 0.0$, and $\delta_3 = -0.16$. Even though all protons have initiated their motion to the acceptor oxygen, proton 2 (shared among Wat25-Ser205) is the one that is ahead, while proton 1 (shared among Cro-Wat25) is the one that lags behind. In the process of going from reactants in S_1 to the transition state structure a noticeable shortening of all hydrogen bonds is noticed: $\Delta d_{AB} = -0.06$, $\Delta d_{BC} = -0.12$, and $\Delta d_{CD} = -0.09$. Thus, summarizing, from a purely topological point of view (i.e., without considering dynamics of the nuclei), the changes brought up by the operation of the proton-wire in S_1 point in the direction of an overall concerted process but where the second proton—that shared among Wat25-Ser205—is

ahead in the transfer, closely followed by the third proton—shared among Ser205-Glu222.

Lastly, when considering the chemical fate of the system in the excited state after photoexcitation, it is important to remember that the photoexcited system does not start off the reactants' minimum in S_1: following Franck—Condon's principle electronic reorganization occurs much faster than nuclear motion. A first-order estimate of the total energy of the system in the excited state right after photoexcitation consists of computing the energy of the structure of the ground-state reactant in S_1. In the current case this yields +85.7 kcal mol^{-1} above the ground-state minimum (see Figure 6). Accepting this value as an acceptable estimate of the energy of the system after photoexcitation, the effective potential energy barrier in S_1 for the 000 → 111 process is reduced to only +0.8 kcal mol^{-1}. The small magnitude of the effective potential energy barrier, combined with the fact that the process involves motion of light nuclei, makes it necessary to include dynamical considerations in the analysis.

3.3.2. Dynamical Corrections. A remarkable consequence of the quantum nature of matter is that bound atoms are never at rest. Thus, the energy values measured in the previous subsection can only be taken as estimations, because they consist only of the Born—Oppenheimer potential energy, that is, nuclei are held fixed in space. A formally correct estimate of the energy differences between different structures must include an estimation of the kinetic energy of the nuclei.

We have computed these dynamical corrections for all chemical entities (structures) present in Figure 6 as follows. In S_1 the only topologically stable (minimum potential energy) structures are reactants (000) and products (111). In these cases, the quantum kinetic energy of the nuclei comes from the vibrational motions of all bound normal modes, which within the harmonic oscillator approximation reads

$$\Delta E_{\text{vibration}} = \frac{1}{2} h \sum_i \nu_i \tag{23}$$

where the summation runs over the six degrees of freedom. The vibrational frequencies ν_i are computed as

$$\nu_i = \frac{1}{2\pi}\sqrt{\lambda_i} \tag{24}$$

where λ_i are the eigenvalues of the mass-weighted Hessian matrix. The transition state structure for the interconversion 000 → 111 in S_1 cannot be treated in the same way because motion is topologically unbound along the reaction coordinate. In this case, the dynamic correction has been computed using eqs 23 and 24 but selecting only the five real frequencies: motion being unbound in one direction means that the Hessian matrix has one negative eigenvalue.

To complete the consideration of dynamical corrections, the question remains as to how to compute them for the Franck—Condon transition. The Franck—Condon principle states that nuclei do not change nuclear motion state in electronic transitions. To compute the dynamical correction to the Franck—Condon transition the nuclear motion wave function needs to be computed. A traditional approach in quantum dynamics simulations mimicks the Franck—Condon transition by promoting the ground vibrational state of the system (i.e., the most populated) in S_0 to the photoactive state. It is possible to determine the ground vibrational state by determining the time evolution in imaginary time (i.e., relaxation) with the S_0 Hamiltonian until invariance in the (imaginary) time-evolved state is achieved, in which case the ground vibrational state is obtained

$$t \to -i\infty \quad \chi(\mathbf{q}) \to \chi_0(\mathbf{q}) \tag{25}$$

where $\chi(\mathbf{q})$ is a reasonable guess (e.g., harmonic oscillator) to the ground-state wave function, and $\chi_0(\mathbf{q})$ the vibrational eigenstate. $\mathbf{q}$ is a vector that defines the nuclear configuration of the system. All that remains is to use an algorithm to solve the time-dependent Schrödinger equation for a multidimensional wave packet $\chi(\mathbf{q})$

$$i\hbar \frac{\partial}{\partial t}\chi(\mathbf{q}, t) = \hat{H}\chi(\mathbf{q}, t) \tag{26}$$

where $\hat{H}$ is the Hamiltonian (total energy) operator for S_0

$$\hat{H}^{S_0} = \hat{T} + \hat{V}^{S_0} \tag{27}$$

Here, $\hat{V}^{S_0}$ is the potential energy surface for the ground electronic state (which is the EVB functional form we have fitted in this work, with parameters shown in Table 2), and $\hat{T}$ is the kinetic energy operator for the system, using the same coordinate set. Recently one of us has published an accurate and successful quantum dynamical simulation of the transfer of an excess proton along a chain of water molecules in which a *linear* model for the complete proton-wire was adopted.[47] The linearity of the model restricted the motion of all atoms in the wire to take place along a line. This assumption effectively halved (at least) the number of degrees of freedom and thus is very appropriate for ulterior dynamical studies. This linear model has also been adopted here and in a related work where the PES presented here has been used.[59] Once the ground-state wave function has been obtained, the *total energy* including dynamical corrections to the Franck—Condon transition is obtained as

$$E_{\text{FC}} = \langle \chi_0 | \hat{H}^{S_1} | \chi_0 \rangle \tag{28}$$

This procedure allows us to obtain a numerically exact (within the bounds of the model) value for the dynamical energy for the ground vibrational state in S_0 or zero-point energy (ZPE) as

$$E_{S_0\,000} = \langle \chi_0 | \hat{H}^{S_0} | \chi_0 \rangle \tag{29}$$

where the Hamiltonian corresponds now to the S_0 electronic state. In this way, a better estimate of the Franck—Condon transition is obtained. To obtain the nuclear motion vibrational ground state $|\chi_0\rangle$ through relaxation dynamics and then to compute E_{FC} (eq 28) and the ZPE for the 000 species in S_0 (eq 29), the Multiconfigurational Time-Dependent Hartree (MCTDH) wave packet propagation method has been used,[63–66] in particular, the Heidelberg MCTDH implementation.[67] The energy results including the dynamical corrections just described are represented also in Figure 6.

The most relevant change from the 'static' picture is the relative energetic ordering of the structures in S_1, because as expected, the small static barrier of +1.9 kcal mol^{-1}

measured from the 000 minimum in S_1 disappears once dynamical corrections are included: the S_1 000 structure is now 4.0 kcal mol^{-1} above the transition state. This means that the 000 species is not stable in S_1. Moreover, after dynamical corrections have been included in the Franck−Condon transition, the initial state in S_1 is now 1.8 kcal mol^{-1} above the 000 structure. The process in the photoactive state is predicted to occur without potential energy barrier.

Conclusions

An EVB-based approach to describe the energetics of operation of heterogeneous proton-wires of arbitrary length has been presented. The PES model described keeps the number of parameters to be fitted to reference data points low, by exploiting the idea of "protonation states," which makes this approach to construct PESes especially suited for long proton-wires.

The method has been used to construct a potential energy function for the ground and photoactive excited states of the three-hydrogen-bond proton-wire in the surroundings of the chromophore of the green fluorescent protein (GFP). This is achieved within a reduced dimensionality model of the EVB method described in this paper, in which the full proton-wire is restricted to remain in a plane and in which each hydrogen bond is restricted to be linear. As reference data, a set of 338 CASPT2//CASSCF energy values for S_0 and S_1 (with an active space of 6 electrons in 6 π molecular orbitals), covering all areas of configurational space relevant to the operation of the proton-wire, has been used. As a result, this paper contains two sets of 56 parameters, one for each electronic state, describing the operation of the proton-wire in GFP.

The fitted PESs have been analyzed in static terms (that is, in terms of stationary points of potential energy). S_0 is seen to contain only a potential energy minimum in the region of reactants. In S_1, besides a deep minimum in the region of photoproducts, a shallow minimum in the area of reactants is also found. Consideration of the Franck−Condon excitation energy (also in static terms) reduces the potential energy barrier to an effective value of only +0.8 kcal mol^{-1}. The transition state structure corresponds to a concerted, though asynchronous, motion of the three protons toward the respective acceptor atoms: the proton of the chromophore is the last to initiate its motion, while the proton of Ser205 at the other end of the proton wire leads the transfer.

Dynamical corrections computed either through the harmonic oscillator approximation or, where possible, through quantum dynamical wave packet relaxation dynamics reveal that the shallow minimum in S_1 in the region of reactants exists only at a purely topological (that is, potential energy) level and that the process is predicted to occur in an essentially barrierless manner in the excited state.

Acknowledgment. The authors are grateful for financial support from the "Ministerio de Educación y Ciencia" and the "Fondo Europeo de Desarrollo Regional" (project CTQ2005-07115/BQU) and from the "Generalitat de Catalunya" (project 2005SGR00400). O.V. acknowledges the European Commission for a Marie Curie individual fellowship.

Supporting Information Available: Table containing the energy of the 338 structures that have been used in the fit and a text file containing the geometrical parameters and energies used in the fit. This material is available free of charge via the Internet at http://pubs.acs.org.

References

(1) Marx, D.; Tuckerman, M.; Hutter, J.; Parrinello, M. *Nature* **1999**, *397*, 601–604.

(2) Warshel, A. In *Computer Modeling of Chemical Reactions in Enzymes and Solutions*; John Wiley and Sons: New York, U.S.A., 1991; pp 1−236.

(3) Åqvist, J.; Warshel, A. *Chem. Rev.* **1993**, *93*, 2523–2544.

(4) Warshel, A. *Annu. Rev. Biophys. Biomol. Struct.* **2003**, *32*, 425–443.

(5) Åqvist, J.; Warshel, A. *J. Mol. Biol.* **1992**, *224*, 7–14.

(6) Pomes, R.; Roux, B. *Biophys. J.* **1996**, *71*, 19–39.

(7) Mei, H. S.; Tuckerman, M. E.; Sagnella, D. E.; Klein, M. L. *J. Phys. Chem. B* **1998**, *102*, 10446–10458.

(8) Decornez, H.; Drukker, K.; Hammes-Schiffer, S. *J. Phys. Chem. A* **1999**, *103*, 2891–2898.

(9) Brewer, M. L.; Schmitt, U. W.; Voth, G. A. *Biophys. J.* **2000**, *78*, 331A–331A.

(10) Brewer, M. L.; Schmitt, U. W.; Voth, G. A. *Biophys. J.* **2001**, *80*, 1691–1702.

(11) Pomes, R.; Roux, B. *Biophys. J.* **2002**, *82*, 2304–2316.

(12) Burykin, A.; Warshel, A. *Biophys. J.* **2003**, *85*, 3696–3706.

(13) Mann, D. J.; Halls, M. D. *Phys. Rev. Lett.* **2003**, *90*, 195503.

(14) Tanner, C.; Manca, C.; Leutwyler, S. *Science* **2003**, *302*, 1736–1739.

(15) Manca, C.; Tanner, C.; Coussan, S.; Bach, A.; Leutwyler, S. *J. Chem. Phys.* **2004**, *121*, 2578–2590.

(16) Braun-Sand, S.; Strajbl, M.; Warshel, A. *Biophys. J.* **2004**, *87*, 2221–2239.

(17) Agmon, N. *Biophys. J.* **2005**, *88*, 2452–2461.

(18) Vendrell, O.; Gelabert, R.; Moreno, M.; Lluch, J. M. *J. Am. Chem. Soc.* **2006**, *128*, 3564–3574.

(19) Kato, M.; Pisliakov, A. V.; Warshel, A. *Proteins* **2006**, *64*, 829–844.

(20) Riccardi, D.; König, P.; Guo, H.; Cui, Q. *Biochemistry* **2008**, *47*, 2369–2378.

(21) Boyer, P. D. *Annu. Rev. Biochem.* **1997**, *66*, 717–749.

(22) Pinto, L. H.; Lamb, R. A. *Photochem. Photobiol. Sci.* **2006**, *5*, 629–632.

(23) Pinto, L. H.; Lamb, R. A. *J. Biol. Chem.* **2006**, *281*, 8997–9000.

(24) Schumacher, K. *Curr. Opin. Plant Biol.* **2006**, *9*, 595–600.

(25) Busenlehner, L. S.; Salomonsson, L.; Brzezinski, P.; Armstrong, R. N. *Proc. Natl. Acad. Sci. U.S.A.* **2006**, *103*, 15398–15403.

(26) Granucci, G.; Hynes, J. T.; Millié, P.; Tran-Thi, T.-H. *J. Am. Chem. Soc.* **2000**, *122*, 12243–12253.

(27) Domcke, W.; Sobolewski, A. L. *Science* **2003**, *302*, 1693–1694.

(28) Mohammed, O. F.; Pines, D.; Dreyer, J.; Pines, E.; Nibbering, E. T. J. *Science* **2005**, *310*, 83–86.

(29) Gelabert, R.; Moreno, M.; Lluch, J. M. *Chem. Phys. Chem.* **2004**, *5*, 1372–1378.

(30) Ortiz-Sánchez, J. M.; Gelabert, R.; Moreno, M.; Lluch, J. M. *J. Phys. Chem. A* **2006**, *110*, 4649–4656.

(31) Ortiz-Sánchez, J. M.; Gelabert, R.; Moreno, M.; Lluch, J. M. *Chem. Phys. Chem.* **2007**, *8*, 1199–1206.

(32) Ortiz-Sánchez, J. M.; Gelabert, R.; Moreno, M.; Lluch, J. M. *J. Chem. Phys.* **2007**, *127*, 084318.

(33) Vendrell, O.; Moreno, M.; Lluch, J. M.; Hammes-Schiffer, S. *J. Phys. Chem. B* **2004**, *108*, 6616–6623.

(34) Luecke, H.; Schobert, B.; Cartailler, J. P.; Richter, H. T.; Rosengarth, A.; Needleman, R.; Lanyi, J. K. *J. Mol. Biol.* **2000**, *300*, 1237–1255.

(35) Zimmer, M. *Chem. Rev.* **2002**, *102*, 759–781.

(36) Schäfer, L. V.; Groenhof, G.; Klingen, A. R.; Ullmann, G. M.; Boggio-Pasqua, M.; Robb, M. A.; Grubmüller, H. *Angew. Chem., Int. Ed.* **2007**, *119*, 536–542.

(37) Balint-Kurti, G. G.; Dixon, R. N.; Marston, C. C. *J. Chem. Soc., Faraday Trans.* **1990**, *86*, 1741–1749.

(38) Tuckerman, M. E.; Marx, D.; Klein, M. L.; Parrinello, M. *J. Chem. Phys.* **1996**, *104*, 5579–5588.

(39) Marx, D.; Hutter, J. Chapter 13. In *Ab Initio Molecular Dynamics: Theory and Implementation*; Grotendorst, J., Ed.; John von Neumann Institut für Computing: Jülich, Germany, 2000; pp 329−477.

(40) Ojamäe, L.; Shavitt, I.; Singer, S. J. *J. Chem. Phys.* **1998**, *109*, 5547–5564.

(41) Warshel, A.; Weiss, R. M. *J. Am. Chem. Soc.* **1980**, *102*, 6218–6226.

(42) Gao, J. L.; Garcia-Viloca, M.; Poulsen, T. D.; Mo, Y. R. *Adv. Phys. Org. Chem.* **2003**, *38*, 161–181.

(43) Mo, Y. R.; Gao, J. L. *J. Comput. Chem.* **2000**, *21*, 1458–1469.

(44) Mo, Y. R.; Gao, J. L. *J. Phys. Chem. A* **2000**, *104*, 3012–3020.

(45) Meyer, H.-D.; Worth, G. A. *Theor. Chim. Acta* **2003**, *109*, 251–267.

(46) Vendrell, O.; Moreno, M.; Lluch, J. M. *J. Chem. Phys.* **2002**, *117*, 7525–7533.

(47) Vendrell, O.; Meyer, H.-D. *J. Chem. Phys.* **2005**, *122*, 104505.

(48) Ward, W. W.; Cody, C. W.; Hart, R. C.; Cormier, M. J. *Photochem. Photobiol.* **1980**, *31*, 611–615.

(49) Morise, H.; Shimomura, O.; Johnson, F. H.; Winant, J. *Biochemistry* **1974**, *13*, 2656–2662.

(50) Kummer, A. D.; Kompa, C.; Lossau, H.; Pollinger-Dammer, F.; Michel-Beyerle, M. E.; Silva, C. M.; Bylina, E. J.; Coleman, W. J.; Yang, M. M.; Youvan, D. C. *Chem. Phys.* **1998**, *237*, 183–193.

(51) Shimomura, O. *FEBS Lett.* **1979**, *104*, 220–222.

(52) Cody, C. W.; Prasher, D. C.; Westler, W. M.; Prendergast, F. G.; Ward, W. W. *Biochemistry* **1993**, *32*, 1212–1218.

(53) Niwa, H.; Inouye, S.; Hirano, T.; Matsuno, T.; Kojima, S.; Kubota, M.; Ohashi, M.; Tsuji, F. I. *Proc. Natl. Acad. Sci. U.S.A.* **1996**, *93*, 13617–13622.

(54) Yang, F.; Moss, L. G.; Phillips, G. N. *Nat. Biotechnol.* **1996**, *14*, 1246–1251.

(55) van Thor, J. J.; Zanetti, G.; Ronayne, K. L.; Towrie, M. *J. Phys. Chem. B* **2005**, *109*, 16099–16108.

(56) Stoner-Ma, D.; Jaye, A. A.; Matousek, P.; Towrie, M.; Meech, S. R.; Tonge, P. J. *J. Am. Chem. Soc.* **2005**, *127*, 2864–2865.

(57) Brejc, K.; Sixma, T. K.; Kitts, P. A.; Kain, S. R.; Tsien, R. Y.; Ormö, M.; Remington, S. J. *Proc. Natl. Acad. Sci. U.S.A.* **1997**, *94*, 2306–2311.

(58) Vendrell, O.; Gelabert, R.; Moreno, M.; Lluch, J. M. *Chem. Phys. Lett.* **2004**, *396*, 202–207.

(59) Vendrell, O.; Gelabert, R.; Moreno, M.; Lluch, J. M. *J. Phys. Chem. B* **2008,** *112*, 5500–5511.

(60) Cembran, A.; Gao, J. *Theor. Chem. Acc.* **2007**, *118*, 211–218.

(61) Schmitt, U. W.; Voth, G. A. *J. Phys. Chem. B* **1998**, *102*, 5547–5551.

(62) Press, W. H.; Flannery, B. P.; Teukolsky, S. A.; Vetterling, W. T. Minimization or Maximization of Functions. In *Numerical Recipes in Fortran*, 2nd ed.; Cambridge University Press: Cambridge, U.K., 1992; pp 387−448.

(63) Meyer, H.-D.; Manthe, U.; Cederbaum, L. S. *Chem. Phys. Lett.* **1990**, *165*, 73–78.

(64) Manthe, U.; Meyer, H.-D.; Cederbaum, L. S. *J. Chem. Phys.* **1992**, *97*, 3199–3213.

(65) Beck, M. H.; Jäckle, A.; Worth, G. A.; Meyer, H.-D. *Phys. Rep.* **2000**, *324*, 1–105.

(66) Meyer, H.-D.; Worth, G. A. *Theor. Chem. Acc.* **2003**, *109*, 251–267.

(67) Worth, G. A.; Beck, M. H.; Jäckle, A.; Meyer, H.-D. The MCTDH Package, Version 8.2 (2000). H.-D. Meyer, Version 8.3 (2002). See http://www.pci.uni-heidelberg.de/tc/usr/mctdh (accessed Apr 18, 2008).

CT800075W